

# Unconventional Superconducting Pairing Symmetries in $\text{La}_3\text{Ni}_2\text{O}_7$ : from the Perspective of Topology

Guan-Hao Feng,<sup>1,\*</sup> Jun Quan,<sup>2,1,†</sup> and Yusheng Hou<sup>3</sup>

<sup>1</sup>*School of Physical Science and Technology, Lingnan Normal University, Zhanjiang, 524048, China*

<sup>2</sup>*School of Physics, Changchun Normal University, Changchun, 130032, China*

<sup>3</sup>*Guangdong Provincial Key Laboratory of Magnetoelectric Physics and Devices,*

*Center for Neutron Science and Technology, School of Physics,*

*Sun Yat-Sen University, Guangzhou, 510275, China*

(Dated: June 10, 2025)

The recently discovered superconductor  $\text{La}_3\text{Ni}_2\text{O}_7$  has attracted significant attention due to its remarkably high  $T_c$  and unconventional pairing mechanism. High-pressure experiments have demonstrated that the emergence of the superconducting phase is associated with a transition to a higher-symmetry structure. Motivated by this observation, we investigate the superconductivity in  $\text{La}_3\text{Ni}_2\text{O}_7$  under high pressure from the perspectives of symmetry and topology. Based on a bilayer two-orbital model with  $\text{Ni-}d_{3z^2-r^2}$  and  $d_{x^2-y^2}$  orbitals, we systematically examine all symmetry-allowed multi-orbital superconducting pairings at the Bogoliubov-de Gennes (BdG) mean-field level, including terms up to next-nearest neighbors. By solving the self-consistent gap equations and analyzing the BdG condensation energies, we find that the  $A_{1g}$  pairing channel is the most probable one. The dominant pairing is  $s_{\pm}$ -wave, originating from the intra-orbital interaction of the bilayer  $\text{Ni-}d_{3z^2-r^2}$  orbital, while the subdominant pairing is  $d_{x^2-y^2}$ -wave, arising from the inter-orbital interactions between the  $d_{3z^2-r^2}$  and  $d_{x^2-y^2}$  orbitals. Furthermore, we implement the theory of symmetry indicator (SI) to reveal the topological characteristics of each pairing channel, demonstrating that the pairing symmetries can be identified by their distinct topological features.

**Introduction.**— The bilayer Ruddlesden-Popper compound  $\text{La}_3\text{Ni}_2\text{O}_7$  exhibits a high onset superconducting transition temperature ( $T_c \approx 80$  K) under moderate pressures, which has recently attracted significant attention [1–21]. Comprehensive high-pressure experiments up to 104 GPa have revealed that the superconducting transition is accompanied by a structural transition from  $A_{mm}$  to  $I4/mmm$  above 10 GPa [16, 17, 22]. The superconducting pairing symmetry and mechanism related to this structural transition remain a major challenge in uncovering the origin of the remarkably high  $T_c$ . Nevertheless, experimental investigations into the properties of the superconductivity have provided some clues to this problem. First, the high  $T_c$  exhibits remarkable robustness under applied magnetic fields and remains unaffected by the low superconducting volume fraction [12–20]. This implies a short superconducting coherence length. Second, no evidence of long-range magnetic order was observed in powder neutron diffraction measurements [4, 23]. This suggests that time-reversal symmetry (TRS) is likely preserved, or that only minor magnetic moments may exist. Third, the maximum superconducting volume fraction reported is approximately 48%, indicating that superconductivity originates from the bilayer  $\text{La}_3\text{Ni}_2\text{O}_7$  phase [17]. Fourth, samples of varying quality exhibit a linear- $T$  dependence of resistivity, which is typically regarded as a signature of strong electronic correlations and suggests an unconventional nature of superconductivity [12, 20, 24].

Based on the experimental findings described above, various theories have been proposed to elucidate the underlying pairing mechanism. Numerous theories suggest

that strong vertical inter-layer antiferromagnetic interactions between the bilayer  $\text{Ni-}d_{3z^2-r^2}$  orbitals drive the superconductivity [25–30]. In these scenarios, Cooper pairs predominantly form on the  $\text{Ni-}d_{3z^2-r^2}$  orbitals, which are associated with the  $\gamma$ -sheet of the Fermi surface, while other models attribute the pairing to the  $\alpha$  and  $\beta$  bands [29, 31–33]. A variety of theoretical approaches, such as functional renormalization group calculations, random phase approximation, and mean-field theory, have been employed. The resulting possible pairing symmetries are believed to be  $s_{\pm}$  [25, 28, 30, 34–42] and  $d$ -wave [29, 31–33, 43–47]. However, at the BdG mean-field level, a specific self-consistent solution converging to a symmetry-allowed form is still lacking. It is therefore important to ask whether this multi-orbital unconventional superconductor can be understood within the BdG mean-field theory as the anisotropic pairings in cuprate and iron-based superconductors.

In this Letter, we systematically investigate the possible superconducting pairing symmetries at the BdG mean-field level. Given that experiments indicate a short superconducting coherence length, we consider candidate superconducting pairings up to next-nearest-neighbor terms. The bilayer  $\text{La}_3\text{Ni}_2\text{O}_7$  under high pressure is expected to respect the symmetries of the non-magnetic Type-II LG  $p4/mmm1'$ , which can be subduced from  $I4/mmm1'$ . Thus, all symmetry-allowed pairings can be identified by the numerical methods with the Qsymm software package [48]. By solving the self-consistent BCS gap equation and analyzing the BdG condensation energy, we demonstrate that the most probable pairing channel is  $A_{1g}$ , with a dominant  $s_{\pm}$ -wave character and a

competing subdominant  $d_{x^2-y^2}$ -wave component. Moreover, we employ theory of SI [49–58] to investigate the topological features induced by the possible unconventional pairing symmetries. Our results support the BdG mean-field theory for bilayer  $\text{La}_3\text{Ni}_2\text{O}_7$  under high pressure.

**Model.**— To illustrate the idea, we begin with the crystal structure of  $\text{La}_3\text{Ni}_2\text{O}_7$  under high pressure from the recent experiments. We construct a two-orbital ( $\text{Ni}-d_{3z^2-r^2}$  and  $d_{x^2-y^2}$ ) convention-II tight-binding model on a bilayer square lattice, respecting the symmetries of Type-II LG  $p4/mmm1'$ . This model is derived via Wannier downfolding of the DFT+U band structure and given by

$$\begin{aligned}
\mathcal{H}_{\mathbf{k}} - \mu &= (\epsilon^z + 2t_1^z (\cos k_x + \cos k_y)) \\
&+ 4t_2^z \cos k_x \cos k_y \rho_0 \frac{\sigma_0 + \sigma_z}{2} s_0 \\
&+ (\epsilon^x + 2t_1^x (\cos k_x + \cos k_y)) \\
&+ 4t_2^x \cos k_x \cos k_y \rho_0 \frac{\sigma_0 - \sigma_z}{2} s_0 \\
&+ 2t_3^z (-\cos k_x + \cos k_y) \rho_0 \sigma_x s_0 \\
&+ (2t_{\perp}^x (\cos k_x + \cos k_y) + \epsilon_{\perp}^x) \rho_x \frac{\sigma_0 + \sigma_z}{2} s_0 \\
&+ 2t_4^z (-\cos k_x + \cos k_y) \rho_x \sigma_x s_0 \\
&+ \epsilon_{\perp}^z \rho_x \frac{\sigma_0 - \sigma_z}{2} s_0,
\end{aligned} \tag{1}$$

where  $\rho_i$ ,  $\sigma_i$ , and  $s_i$  ( $i = 0, x, y, z$ ) are the Pauli matrices for the layer, orbital, and spin degrees of freedom, respectively. The basis operator used here is  $\psi_{\mathbf{k}\sigma}^{\dagger} = [c_{Az\uparrow}^{\dagger}, c_{Az\downarrow}^{\dagger}, c_{Ax\uparrow}^{\dagger}, c_{Ax\downarrow}^{\dagger}, c_{Bz\uparrow}^{\dagger}, c_{Bz\downarrow}^{\dagger}, c_{Bx\uparrow}^{\dagger}, c_{Bx\downarrow}^{\dagger}]$ , where  $A$  and  $B$  label the bilayer, and  $x$  and  $z$  denote  $d_{x^2-y^2}$  and  $d_{3z^2-r^2}$  orbital, respectively. We have adopted the conventional lattice basis here and considered up to the next-nearest-neighbor hoppings, since the resulting Fermi surface is sufficient to capture the topological properties of the superconducting system, as shown in Fig. 1(a). The parameter values of this normal-state Hamiltonian are provided in Supplementary Note 17 [59]. This minimal two-orbital model closely follows that of Luo et al. [60], and we adopt the same parameter notation here. However, we consider an effective Hubbard  $U = 3.5$  eV to account for the correlation effects of the  $3d$  electrons in the Ni atoms.

In the absence of long-range magnetic order, as evidenced by neutron diffraction and inelastic neutron scattering experiments down to a temperature of 10 K [4, 23], the superconducting pairing is believed to arise from spin fluctuations [29, 40, 42]. These strong interactions should be effectively attractive and preserve the symmetries of non-magnetic LG  $p4/mmm1'$ . Thus, we introduce the extended multi-orbital attractive Hubbard interactions,

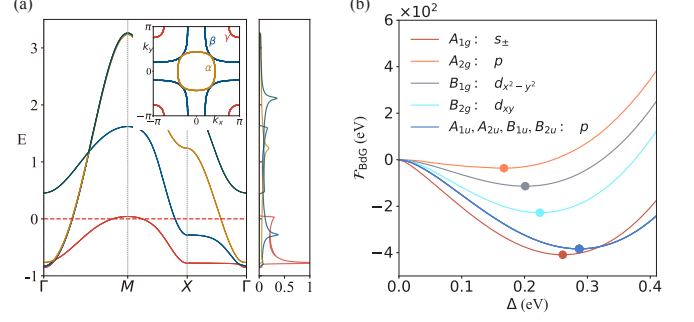


Figure 1. (a) Band structure of the bilayer tight-binding model in Eq. 1. The subfigures show the Fermi surface and the normalized DOS of each band. (b) Comparison of BdG condensation energies of the dominant pairings across the eight real one-dimensional representation pairing channels. The point inside each curve is the saddle-point solution of the corresponding BCS gap equation.

which take a factorizable form,

$$H_{\text{attr}} = \sum_{\mathbf{k}\mathbf{k}'\alpha\beta s s'} V_{\text{eff}} c_{\mathbf{k}\alpha s}^{\dagger} c_{-\mathbf{k}\beta s'}^{\dagger} c_{-\mathbf{k}'\beta s'} c_{\mathbf{k}'\alpha s}, \tag{2}$$

where  $V_{\text{eff}} = \frac{-V_{\alpha\beta s s'}}{N} e^{-i(\mathbf{k}-\mathbf{k}')\cdot\mathbf{r}_{\alpha\beta s s'}}$ , with  $s$  and  $s'$  representing the spin degrees of freedom, while  $\alpha$  and  $\beta$  denoting the degrees of freedom other than spin. Here,  $N$  is the number of discrete momentum points  $\mathbf{k}$  (or  $\mathbf{k}'$ );  $V_{\alpha\beta s s'}$  is the strength of the attractive potential; and the phase factor  $e^{-i(\mathbf{k}-\mathbf{k}')\cdot\mathbf{r}_{\alpha\beta s s'}}$  arises from the Fourier transform of the Cooper pair creation operator  $c_{\mathbf{k}\alpha s}^{\dagger} c_{-\mathbf{k}\beta s'}^{\dagger}$  and annihilation operator  $c_{-\mathbf{k}'\beta s'} c_{\mathbf{k}'\alpha s}$ . We then carry out the Hubbard–Stratonovich decoupling [59] and obtain the mean-field pairing potential

$$\begin{aligned}
H_{\text{attr}}^{\text{MF}} &= H_{\Delta} + \sum_{\alpha\beta s s'} \frac{N}{V_{\alpha\beta s s'}} \Delta_{\alpha\beta s s'}^* \Delta_{\alpha\beta s s'} \\
H_{\Delta} &= \sum_{\mathbf{k}\alpha\beta s s'} (\Delta_{\alpha\beta s s'}^* e^{i\mathbf{k}\cdot\mathbf{r}_{\alpha\beta}} c_{-\mathbf{k}\beta s'} c_{\mathbf{k}\alpha s} \\
&+ \Delta_{\alpha\beta s s'} e^{-i\mathbf{k}\cdot\mathbf{r}_{\alpha\beta}} c_{\mathbf{k}\alpha s}^{\dagger} c_{-\mathbf{k}\beta s'}^{\dagger}).
\end{aligned} \tag{3}$$

The combination of the terms  $\Delta_{\alpha\beta s s'}^* e^{i\mathbf{k}\cdot\mathbf{r}_{\alpha\beta s s'}}$  in  $H_{\Delta}$  can result in various pairing symmetries, including  $s_{\pm}$ ,  $p_x \pm ip_y$ ,  $d_{x^2-y^2}$ , and  $d_{xy}$ . The favored pairing symmetry is then determined by the free energy using the standard expression [59, 61, 62]

$$\mathcal{F}_S = \frac{Nn}{V} |\Delta|^2 - 2k_B T \sum_{\mathbf{k}\alpha} \ln [2 \cosh(\beta E_{\mathbf{k}\alpha}^{\text{BdG}}/2)], \tag{5}$$

where the energy eigenvalues of the BdG Hamiltonian are denoted as  $\pm E_{\mathbf{k}\alpha}^{\text{BdG}}$ , and  $\beta = 1/k_B T$  is the inverse temperature. The elements  $\Delta_{\alpha\beta s s'}$  with the same value  $\Delta$  together form the pairing gap matrix  $\tilde{\Delta}$  in the Nambu basis. Here,  $n$  is the number of nonzero elements in  $\tilde{\Delta}$ .

When  $\Delta = 0$ , Eq. 5 reduces to the normal-state free energy  $\mathcal{F}_N$ . The equilibrium gap value  $\Delta = \Delta_{\alpha\beta ss'}$  can be identified by minimizing  $\mathcal{F}_S$  with respect to  $\Delta^*$ , which leads to the self-consistent BCS gap equation

$$\Delta = -\frac{V}{Nn} \sum_{\mathbf{k}} \text{Tr} \left[ \frac{\partial \mathcal{H}_{\mathbf{k}}^{\text{BdG}}}{\partial \Delta} U_{\mathbf{k}} n_F(E_{\mathbf{k}}^{\text{BdG}}) U_{\mathbf{k}}^\dagger \right], \quad (6)$$

where  $n_F$  is a diagonal matrix whose entries are the Fermi distribution functions for the eigenvalues  $E_{\mathbf{k}}^{\text{BdG}}$ . Here  $U_{\mathbf{k}}$  is the unitary matrix that diagonalizes the BdG Hamiltonian. The favored pairing symmetry can be determined by comparing the BCS condensation energies,  $\mathcal{F}_{\text{BdG}} = \mathcal{F}_S - \mathcal{F}_N$ .

When considering pairings up to the next-nearest neighbors, the number of the symmetry-allowed pairings  $H_\Delta$  is limited, which can be systematically identified using the numerical methods with the generators of BdG Hamiltonian in different pairing channels [59] and the Qsymm software package [48]. The favored pairing states can subsequently be determined by solving the self-consistent gap equations in Eq. 6 and performing a BdG condensation energy analysis with Eq. 5, as summarized in Tab. I.

**Topological Classification.**- In light of the difficulties in experimentally realizing class CII ( $\mathcal{P}^2 = -1$ ) superconducting states in electronic systems [63], we restrict our analysis to class DIII ( $\mathcal{P}^2 = +1$ ) in the Altland-Zirnbauer (AZ) ten-fold way classification. Under high pressure, the crystal structure of bilayer  $\text{La}_3\text{Ni}_2\text{O}_7$  exhibits the symmetries of Type-II LG  $p4/mmm1'$ . The corresponding point group is  $4/mmm (D_{4h})$ , which possesses eight real 1D and two 2D representations. Since the TRS is preserved in the superconducting phase, the pairings must belong to one of the 1D pairing channels of  $A_{1g}$ ,  $A_{2g}$ ,  $B_{1g}$ ,  $B_{2g}$ ,  $A_{1u}$ ,  $A_{2u}$ ,  $B_{1u}$ , and  $B_{2u}$  [64–66].

In the presence of inversion symmetry, the band can also be classified according to the AZ+I classification [67]. Note that the even-parity pairing channels satisfy the commutation relation  $[\mathcal{P}, \mathcal{I}] = 0$ , which leads to  $(\mathcal{P}\mathcal{I})^2 = +1$ . These systems fall into class DIII, supporting topologically protected  $2\mathbb{Z}$  nodal points [67]. In contrast, the odd-parity pairing channel satisfies the anticommutation relation  $\{\mathcal{P}, \mathcal{I}\} = 0$ , resulting in  $(\mathcal{P}\mathcal{I})^2 = -1$ , and such systems fall into class CII without topological nodes.

For the bands satisfying the insulating compatibility relations of Type-II LG  $p4/mmm1'$ , the original SI group is  $X_{\text{BS}} = \mathbb{Z}_4$  [59]. The original SIs can also be used to indicate topological superconducting states by neglecting particle-hole symmetry (PHS). However, the presence of PHS implies that the topological properties of superconducting states should be determined by both positive and negative-energy quasiparticles. Since the symmetry indicators are linear functions of the symmetry data vectors of the bands, the overall band topology can be regarded

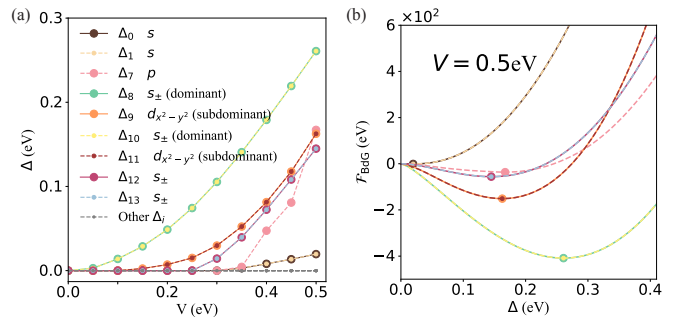


Figure 2. (a) Pairing strength  $\Delta_i$  vs  $V_i$  obtained by solving the self-consistent BCS gap equations Eq. 6 in the  $A_{1g}$  pairing channel. (b) BdG condensation energy  $\mathcal{F}_{\text{BdG}}$  vs  $|\Delta_i|$  at  $V_i = 0.5$  eV. The result verifies that the values of  $|\Delta_i|$  in (a) are do the saddle points of the corresponding BdG condensation energy. The comparison shows that the  $s_{\pm}$ -wave pairings are dominant, while the  $d_{x^2-y^2}$ -wave pairings are subdominant.

as a stacking of the topological properties of individual bands that satisfy the insulating compatibility relations. In this way, the two bands closest to  $E = 0$  determine whether the quasiparticle spectrum is gapped or gapless, i.e.,  $z_4^{\text{nodal}} = z_4^{(1)} + \bar{z}_4^{(1)} \pmod{4}$ ; while the other bands determine the edge states, i.e.,  $z_4^{\text{edge}} = z_4 - z_4^{\text{nodal}} \pmod{4}$ . Here  $z_4^{(1)}$  and  $\bar{z}_4^{(1)}$  is the original SI for the first band below and above  $E = 0$ , respectively.

The theory of original SI may have difficulty in identifying higher-order TSC phases. Alternatively, the refined SI provides a reliable approach to address this limitation [63, 68]. Therefore, for completeness, we also calculate the refined SIs. For the  $A_{1g}/A_{2g}$  pairing channels, the refined SI group is trivial; For the  $B_{1g}/B_{2g}$  pairing channels, the refined SI group is  $X_{\text{BS}}^{\text{BdG}} = \mathbb{Z}_2 \times \mathbb{Z}_2$ , while for the  $A_{1u}/A_{2u}$  and  $B_{1u}/B_{2u}$  pairing channels, the refined SI groups are both  $X_{\text{BS}}^{\text{BdG}} = \mathbb{Z}_2 \times \mathbb{Z}_8$ . The results of topological classification are summarized in Supplementary Note 3 [59].

**Nodal superconducting phases.**- According to the AZ+I classification, the even-parity pairing channels,  $A_{1g}$ ,  $A_{2g}$ ,  $B_{1g}$ , and  $B_{2g}$ , support topological nodal points, which are characterized by a  $2\mathbb{Z}$ -valued  $\pi_1$ -charge corresponding to the usual winding number.

For the  $A_{1g}$  pairing channel, we found that only 15 kinds of mean-field pairing potentials are permissible. The dominant pairings are  $s_{\pm}$ -wave symmetric, as shown in Fig. 2. The Pauli matrix structures with  $\sigma_0 + \sigma_z$  suggest that the pairings originate from the effectively attractive intra-orbital interactions of the electrons within the bilayer  $d_{3z^2-r^2}$  orbitals. The BdG condensation energy of the dominant  $s_{\pm}$ -wave pairings is the lowest compared to any other pairing channels, as shown in Fig. 1(b). Therefore, we conclude that the  $A_{1g}$  pairing channel is the most probable one. Moreover, the subdominant pairing symmetry is  $d_{x^2-y^2}$ -wave symmetric. The

Table I. The dominant and subdominant pairings in different channels.

$4/mmm(D_{4h})$	Dominant	Subdominant
$A_{1g}$	$\Delta_8 [(\cos k_x + \cos k_y) \tau_y \rho_0 (\sigma_0 + \sigma_z) s_y]$ $\Delta_{10} [(\cos k_x + \cos k_y) \tau_y \rho_x (\sigma_0 + \sigma_z) s_y]$	$2\Delta_9 [(\cos k_x - \cos k_y) \tau_y \rho_0 \sigma_x s_y]$ $2\Delta_{11} [(\cos k_x - \cos k_y) \tau_y \rho_x \sigma_x s_y]$
$A_{2g}$	$\Delta_3 [\sin k_x \tau_x \rho_z (\sigma_0 - \sigma_z) s_z + \sin k_y \tau_y \rho_z (\sigma_0 - \sigma_z) s_0]$	$4\Delta_6 \sin k_x \sin k_y \tau_y \rho_0 \sigma_x s_y$ $4\Delta_7 \sin k_x \sin k_y \tau_y \rho_x \sigma_x s_y$
$B_{1g}$	$\Delta_6 [(\cos k_x - \cos k_y) \tau_y \rho_0 (\sigma_0 + \sigma_z) s_y]$ $\Delta_8 [(\cos k_x - \cos k_y) \tau_y \rho_x (\sigma_0 + \sigma_z) s_y]$	$\Delta_{10} [(\cos k_x - \cos k_y) \tau_y \rho_0 (\sigma_0 - \sigma_z) s_y]$ $\Delta_{11} [(\cos k_x - \cos k_y) \tau_y \rho_x (\sigma_0 - \sigma_z) s_y]$
$B_{2g}$	$2\Delta_8 \sin k_x \sin k_y \tau_y \rho_0 (\sigma_0 + \sigma_z) s_y$ $2\Delta_9 \sin k_x \sin k_y \tau_y \rho_x (\sigma_0 + \sigma_z) s_y$	$2\Delta_{10} \sin k_x \sin k_y \tau_y \rho_0 (\sigma_0 - \sigma_z) s_y$ $2\Delta_{11} \sin k_x \sin k_y \tau_y \rho_x (\sigma_0 - \sigma_z) s_y$
$A_{1u}$	$\Delta_2 [\sin k_x \tau_x \rho_0 (\sigma_0 + \sigma_z) s_z + \sin k_y \tau_y \rho_0 (\sigma_0 + \sigma_z) s_0]$ $\Delta_4 [\sin k_x \tau_x \rho_x (\sigma_0 + \sigma_z) s_z + \sin k_y \tau_y \rho_x (\sigma_0 + \sigma_z) s_0]$	$\Delta_6 [\sin k_x \tau_x \rho_0 (\sigma_0 - \sigma_z) s_z + \sin k_y \tau_y \rho_0 (\sigma_0 - \sigma_z) s_0]$ $\Delta_7 [\sin k_x \tau_x \rho_x (\sigma_0 - \sigma_z) s_z + \sin k_y \tau_y \rho_x (\sigma_0 - \sigma_z) s_0]$
$A_{2u}$	$\Delta_2 [\sin k_x \tau_y \rho_0 (\sigma_0 + \sigma_z) s_0 - \sin k_y \tau_x \rho_0 (\sigma_0 + \sigma_z) s_z]$ $\Delta_4 [\sin k_x \tau_y \rho_x (\sigma_0 + \sigma_z) s_0 - \sin k_y \tau_x \rho_x (\sigma_0 + \sigma_z) s_z]$	$\Delta_6 [\sin k_x \tau_y \rho_0 (\sigma_0 - \sigma_z) s_0 - \sin k_y \tau_x \rho_0 (\sigma_0 - \sigma_z) s_z]$ $\Delta_7 [\sin k_x \tau_y \rho_x (\sigma_0 - \sigma_z) s_0 - \sin k_y \tau_x \rho_x (\sigma_0 - \sigma_z) s_z]$
$B_{1u}$	$\Delta_2 [\sin k_x \tau_x \rho_0 (\sigma_0 + \sigma_z) s_z - \sin k_y \tau_y \rho_0 (\sigma_0 + \sigma_z) s_0]$ $\Delta_4 [\sin k_x \tau_x \rho_x (\sigma_0 + \sigma_z) s_z - \sin k_y \tau_y \rho_x (\sigma_0 + \sigma_z) s_0]$	$\Delta_6 [\sin k_x \tau_x \rho_0 (\sigma_0 - \sigma_z) s_z - \sin k_y \tau_y \rho_0 (\sigma_0 - \sigma_z) s_0]$ $\Delta_7 [\sin k_x \tau_x \rho_x (\sigma_0 - \sigma_z) s_z - \sin k_y \tau_y \rho_x (\sigma_0 - \sigma_z) s_0]$
$B_{2u}$	$\Delta_2 [\sin k_x \tau_y \rho_0 (\sigma_0 + \sigma_z) s_0 + \sin k_y \tau_x \rho_0 (\sigma_0 + \sigma_z) s_z]$ $\Delta_4 [\sin k_x \tau_y \rho_x (\sigma_0 + \sigma_z) s_0 + \sin k_y \tau_x \rho_x (\sigma_0 + \sigma_z) s_z]$	$\Delta_6 [\sin k_x \tau_y \rho_0 (\sigma_0 - \sigma_z) s_0 + \sin k_y \tau_x \rho_0 (\sigma_0 - \sigma_z) s_z]$ $\Delta_7 [\sin k_x \tau_y \rho_x (\sigma_0 - \sigma_z) s_0 + \sin k_y \tau_x \rho_x (\sigma_0 - \sigma_z) s_z]$

off-diagonal matrix  $\sigma_x$  in the Pauli matrix structures implies that the subdominant pairings arise from the inter-orbital interactions between the  $d_{3z^2-r^2}$  and  $d_{x^2-y^2}$  orbitals. This result suggests a competitive relationship between the  $s_{\pm}$ - and  $d_{x^2-y^2}$ -wave pairings, in accordance with the results in Refs. [25, 70]. This pairing channel is topologically trivial [71], with the original SI  $z_4 = 0$  and a trivial refined SI group. However, this does not necessarily imply that the system must exhibit a band gap. Accidental band nodes may still arise, and while some of these nodes can even carry topological charges, it is crucial to emphasize that not all do. In the presence of the dominant and subdominant pairings, accidental band nodes without any associated topological charges can be observed, as shown in Figs. 3 (a) and (e).

For the  $A_{2g}$  pairing channel, only 8 kinds of mean-field pairings are permissible and the dominant pairings exhibit  $p$ -wave symmetry. The Pauli matrix structures with  $\rho_z$  and  $\sigma_0 - \sigma_z$  suggest that the pairings originate from effectively attractive intra-orbital interactions between the electrons within the intra-layer  $d_{x^2-y^2}$  orbitals. In this case, original and refined SIs are both trivial. However, in contrast to  $A_{1g}$ , the  $A_{2g}$  exhibits nontrivial topological property indicated by the  $\mathbb{Z}_2$ -enriched SI in Ref. [72]. Termination along  $x$  or  $y$ -direction shows the coexistence of topological nodal points and the helical Majorana edge states, as shown in Figs. 3(b) and (f). This special topological state can also be well indicated by the nontrivial original SIs  $z_4^{\text{nodal}} = -2$  and

$z_4^{\text{edge}} = +2$ . Moreover, the projected nodal points are connected by flat Majorana edge states, analogous to the nodal points with topological edge states in zigzag ribbons of graphene. This topological feature originates from the characters  $\chi_{C_{2x(y)}} = -1$ , and the sign of  $\tilde{\Delta}$  will be flipped under the  $C_{2x(y)}$  rotation symmetries, i.e.,  $C_{2x(y)} \tilde{\Delta} C_{2x(y)}^T = -\tilde{\Delta}$ . Since the  $\pi_1$  integral path also reverses under  $C_{2x(y)}$  rotation symmetries, the winding numbers of the nodal points related by the  $C_{2x(y)}$  rotation symmetries are identical. Thus the net topological charges will be preserved when the nodal points are projected onto the  $x$  or  $y$ -edges, which leads to the flat Majorana edge states. Despite the presence of the distinctive topological feature, the relatively low BdG condensation energy implies a low likelihood of its realization in experimental settings (see Supplementary Note 10 for details [59]).

For the  $B_{1g}$  pairing channel, we found 12 kinds of mean-field pairings are permissible and the dominant pairings exhibit  $d_{x^2-y^2}$ -wave symmetry. The Pauli matrix structures of the dominant pairings are the same as those in the  $A_{1g}$  pairing channel. The nontrivial refined SIs  $(z_{2,1}, z_{2,2}) = (1, 0)$  indicating this topological nodal superconducting phase, as illustrated in Fig. 3(c). This phase can also be indicated by the original SI  $z_4 = z_4^{\text{nodal}} = -2$ . When the  $x$  or  $y$ -edge is terminated, the projected nodal points carry no net topological charge, and thus no flat Majorana edge states emerge in this scenario, as shown in Fig. 3(g). This nodal band

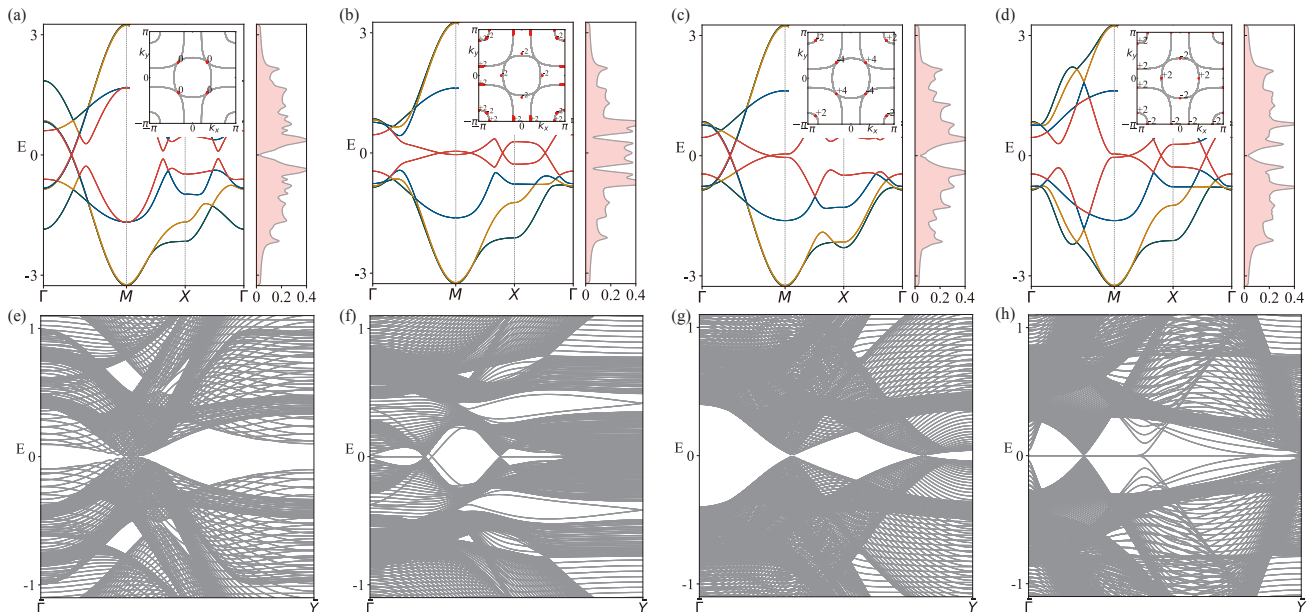


Figure 3. (a)-(d) Nodal bulk spectra of the superconducting states in the  $A_{1g}$ ,  $A_{2g}$ ,  $B_{1g}$ , and  $B_{2g}$  pairing channels, respectively. The subfigures display the locations of the nodal points in the BZ as well as the normalized DOSs. The numbers insight the subfigures represent the values of the winding number. (e)-(h) Corresponding edge spectra when the 2D lattice is terminated in the  $x$  direction. The parameter values employed here are list in Supplementary Notes 9-12 [59]. The figures of band spectra are computed by the PythTB software package [69].

structure comes from the characters  $\chi_{C_{2x(y)}} = +1$ , in contrast to the cases of  $A_{2g}$  and  $B_{2g}$ .

For  $B_{2g}$  pairing channel, we also found that 12 kinds of mean-field pairing potentials are possible. The dominant pairings are  $d_{xy}$ -wave symmetric whose Pauli matrix structures are also identical to those in the  $A_{1g}$  pairing channel. Although the refined SI group  $X_{\text{BS}}^{\text{BdG}}$  is identical to that of the  $B_{1g}$  pairing channel, the edge spectrum under terminations along the  $x$  or  $y$ -direction exhibits nodal points accompanied by flat Majorana edge states, which has been discussed in the case of  $A_{2g}$ . The topological nodal state is also indicated by  $z_4 = z_4^{\text{nodal}} = -2$  and  $(z_{2,1}, z_{2,2}) = (1, 0)$ , as shown in Figs. 3(d) and (h).

**Gapped superconducting phases.**- We found that the dominant pairings in the four odd-parity channels,  $A_{1u}$ ,  $A_{2u}$ ,  $B_{1u}$ , and  $B_{2u}$ , exhibit  $p$ -wave symmetric. The Pauli matrix structures all are relate to  $\sigma_0 + \sigma_z$  implying that they are contributed by the electrons within the bilayer  $d_{3z^2-r^2}$  orbitals. Since the odd-parity pairing channels share the same refined SI group, their topological properties are quite similar. These pairing channels would lead to the gapped topological bulk states with helical Majorana edge states. For the  $A_{1u}/A_{2u}$  channels, we found  $(z_2, z_8) = (0, -3)$  and  $z_4 = z_4^{\text{edge}} = -3$ . For the  $B_{1u}/B_{2u}$  pairing channels, we found  $(z_2, z_8) = (0, 1)$  and  $z_4 = z_4^{\text{edge}} = +3$ . Therefore, the nontrivial-valued  $z_4^{\text{edge}}$  denotes the mirror Chern number, corresponding to three pairs of helical Majorana edge modes in the bulk band gap. Given the BdG condensation energy is slightly

higher than that of the  $A_{1g}$  pairing channel in Fig. 1(b), further experimental evidence is needed to determine the exact pairing symmetry.

**Conclusion and Discussion.**- We have studied the pairing symmetries and the corresponding topological features of  $\text{La}_3\text{Ni}_2\text{O}_7$  under high pressure using BdG mean-field theory. We found that the  $A_{1g}$  pairing channel is the most probable one. The dominant pairing symmetry is  $s_{\pm}$ -wave originating from the attractive electron interaction within the bilayer  $d_{3z^2-r^2}$  orbitals. We also found that the subdominant pairings exhibit  $d_{x^2-y^2}$ -wave symmetry, supporting the results in Refs. [25, 70]. The dominant pairing symmetries in the  $A_{1g}(s_{\pm})$ ,  $B_{1g}(d_{x^2-y^2})$ , and  $B_{2g}(d_{xy})$  channels are in good agreement with the results of the RPA analysis presented in Ref. [43]. Furthermore, we demonstrated that dominant pairings in the  $A_{2g}$ ,  $A_{1u}$ ,  $A_{2u}$ ,  $B_{1u}$ , and  $B_{2u}$  exhibit  $p$ -wave symmetry.

For the all of the possible pairing channels, we have comprehensively studied the relationship between pairing symmetries and topological properties using both the original and refined SI theories. We found that even-parity pairings give rise to nodal topological phases, whereas odd-parity pairings result in gapped topological phases. The distinct topological spectra thus serve as signatures of the underlying pairing symmetries. Our study provides significant insights into the superconducting pairing symmetry and mechanism of  $\text{La}_3\text{Ni}_2\text{O}_7$  under high pressure.

In this work, TRS is assumed to be preserved; there-

fore, possible TRS-breaking pairing symmetries, such as the  $(d + is)$ -wave pairing [29, 32], are excluded from the consideration. The origin of the effectively attractive interactions has been neglected and still requires further investigation into the underlying mechanisms. Following our discussion of the superconducting spectra, experimental techniques such as ARPES, neutron scattering, Hall effect measurements, and scanning tunneling microscopy can provide valuable insights for identifying the pairing symmetries.

Very recently, the experimental superconducting tunneling spectra showed an anisotropic  $s$ -wave structure in the dominant pairing [73]. Pure  $d$ -wave models are not supported. The nonzero conductance near zero bias indicates that it is a nodal gap. These characteristics are quite consistent with our analysis in the  $A_{1g}$  pairing channel.

We thank Zhongbo Yan and Cui-Qun Chen for helpful discussions. G.F. thanks Seishiro Ono for valuable discussions. This work is supported by Guangdong Basic and Applied Basic Research Foundation (Grant No. 2023A1515110002, 2023A1515011796, 2024A1515011908) and the National Natural Sciences Foundation of China (Grant No. 12474247 and 92165204).

---

\* fenggh@lingnan.edu.cn

† quanj@lingnan.edu.cn

- [1] Y. Meng, Y. Yang, H. Sun, S. Zhang, J. Luo, L. Chen, X. Ma, M. Wang, F. Hong, X. Wang, and X. Yu, Density-wave-like gap evolution in  $\text{La}_3\text{Ni}_2\text{O}_7$  under high pressure revealed by ultrafast optical spectroscopy, *Nature Communications* **15**, 10408 (2024).
- [2] Z. Dong, M. Huo, J. Li, J. Li, P. Li, H. Sun, L. Gu, Y. Lu, M. Wang, Y. Wang, and Z. Chen, Visualization of oxygen vacancies and self-doped ligand holes in  $\text{La}_3\text{Ni}_2\text{O}_{7-\delta}$ , *Nature* **630**, 847 (2024).
- [3] B. Chen, H. Zhang, J. Li, D. Hu, M. Huo, S. Wang, C. Xi, Z. Wang, H. Sun, M. Wang, and B. Shen, Unveiling the multiband metallic nature of the normal state in the nickelate  $\text{La}_3\text{Ni}_2\text{O}_7$ , *Physical Review B* **111**, 054519 (2025).
- [4] T. Xie, M. Huo, X. Ni, F. Shen, X. Huang, H. Sun, H. C. Walker, D. Adroja, D. Yu, B. Shen, L. He, K. Cao, and M. Wang, Strong interlayer magnetic exchange coupling in  $\text{La}_3\text{Ni}_2\text{O}_{7-\delta}$  revealed by inelastic neutron scattering, *Science Bulletin* **69**, 3221 (2024).
- [5] X. Ren, R. Sutarto, X. Wu, J. Zhang, H. Huang, T. Xiang, J. Hu, R. Comin, X. Zhou, and Z. Zhu, Resolving the electronic ground state of  $\text{La}_3\text{Ni}_2\text{O}_{7-\delta}$  films, *Communications Physics* **8**, 1 (2025).
- [6] D. Zhao, Y. Zhou, M. Huo, Y. Wang, L. Nie, Y. Yang, J. Ying, M. Wang, T. Wu, and X. Chen, Pressure-enhanced spin-density-wave transition in double-layer nickelate  $\text{La}_3\text{Ni}_2\text{O}_{7-\delta}$ , *Science Bulletin* 10.1016/j.scib.2025.02.019 (2025).
- [7] J. Yang, H. Sun, X. Hu, Y. Xie, T. Miao, H. Luo, H. Chen, B. Liang, W. Zhu, G. Qu, C.-Q. Chen, M. Huo, Y. Huang, S. Zhang, F. Zhang, F. Yang, Z. Wang, Q. Peng, H. Mao, G. Liu, Z. Xu, T. Qian, D.-X. Yao, M. Wang, L. Zhao, and X. J. Zhou, Orbital-dependent electron correlation in double-layer nickelate  $\text{La}_3\text{Ni}_2\text{O}_7$ , *Nature Communications* **15**, 4373 (2024).
- [8] M. Wang, H.-H. Wen, T. Wu, D.-X. Yao, and T. Xiang, Normal and Superconducting Properties of  $\text{La}_3\text{Ni}_2\text{O}_7$ , *Chinese Physics Letters* **41**, 077402 (2024).
- [9] Z. Liu, H. Sun, M. Huo, X. Ma, Y. Ji, E. Yi, L. Li, H. Liu, J. Yu, Z. Zhang, Z. Chen, F. Liang, H. Dong, H. Guo, D. Zhong, B. Shen, S. Li, and M. Wang, Evidence for charge and spin density waves in single crystals of  $\text{La}_3\text{Ni}_2\text{O}_7$  and  $\text{La}_3\text{Ni}_2\text{O}_6$ , *Science China Physics, Mechanics & Astronomy* **66**, 217411 (2022).
- [10] K. Chen, X. Liu, J. Jiao, M. Zou, C. Jiang, X. Li, Y. Luo, Q. Wu, N. Zhang, Y. Guo, and L. Shu, Evidence of spin density waves in  $\text{La}_3\text{Ni}_2\text{O}_{7-\delta}$ , *Phys. Rev. Lett.* **132**, 256503 (2024).
- [11] S. Abadi, K.-J. Xu, E. G. Lomeli, P. Puphal, M. Isobe, Y. Zhong, A. V. Fedorov, S.-K. Mo, M. Hashimoto, D.-H. Lu, B. Moritz, B. Keimer, T. P. Devereaux, M. Hepting, and Z.-X. Shen, Electronic structure of the alternating monolayer-trilayer phase of  $\text{La}_3\text{Ni}_2\text{O}_7$ , *Phys. Rev. Lett.* **134**, 126001 (2025).
- [12] H. Sun, M. Huo, X. Hu, J. Li, Z. Liu, Y. Han, L. Tang, Z. Mao, P. Yang, B. Wang, J. Cheng, D.-X. Yao, G.-M. Zhang, and M. Wang, Signatures of superconductivity near 80 K in a nickelate under high pressure, *Nature* **621**, 493 (2023).
- [13] H. Sakakibara, M. Ochi, H. Nagata, Y. Ueki, H. Sakurai, R. Matsumoto, K. Terashima, K. Hirose, H. Ohta, M. Kato, Y. Takano, and K. Kuroki, Theoretical analysis on the possibility of superconductivity in the trilayer ruddlesden-popper nickelate  $\text{La}_4\text{Ni}_3\text{O}_{10}$  under pressure and its experimental examination: Comparison with  $\text{La}_3\text{Ni}_2\text{O}_7$ , *Phys. Rev. B* **109**, 144511 (2024).
- [14] M. Zhang, C. Pei, Q. Wang, Y. Zhao, C. Li, W. Cao, S. Zhu, J. Wu, and Y. Qi, Effects of pressure and doping on Ruddlesden-Popper phases  $\text{La}_{n+1}\text{Ni}_n\text{O}_{3n+1}$ , *Journal of Materials Science & Technology* **185**, 147 (2024).
- [15] G. Wang, N. N. Wang, X. L. Shen, J. Hou, L. Ma, L. F. Shi, Z. A. Ren, Y. D. Gu, H. M. Ma, P. T. Yang, Z. Y. Liu, H. Z. Guo, J. P. Sun, G. M. Zhang, S. Calder, J.-Q. Yan, B. S. Wang, Y. Uwatoko, and J.-G. Cheng, Pressure-induced superconductivity in polycrystalline  $\text{La}_3\text{Ni}_2\text{O}_{7-\delta}$ , *Phys. Rev. X* **14**, 011040 (2024).
- [16] N. Wang, G. Wang, X. Shen, J. Hou, J. Luo, X. Ma, H. Yang, L. Shi, J. Dou, J. Feng, J. Yang, Y. Shi, Z. Ren, H. Ma, P. Yang, Z. Liu, Y. Liu, H. Zhang, X. Dong, Y. Wang, K. Jiang, J. Hu, S. Nagasaki, K. Kitagawa, S. Calder, J. Yan, J. Sun, B. Wang, R. Zhou, Y. Uwatoko, and J. Cheng, Bulk high-temperature superconductivity in pressurized tetragonal  $\text{La}_2\text{PrNi}_2\text{O}_7$ , *Nature* **634**, 579 (2024).
- [17] J. Li, D. Peng, P. Ma, H. Zhang, Z. Xing, X. Huang, C. Huang, M. Huo, D. Hu, Z. Dong, X. Chen, T. Xie, H. Dong, H. Sun, Q. Zeng, H.-k. Mao, and M. Wang, Identification of superconductivity in bilayer nickelate  $\text{La}_3\text{Ni}_2\text{O}_7$  under high pressure up to 100 GPa, *National Science Review*, nwaf220 (2025).
- [18] Y. Zhou, J. Guo, S. Cai, H. Sun, C. Li, J. Zhao, P. Wang, J. Han, X. Chen, Y. Chen, Q. Wu, Y. Ding, T. Xiang, H.-k. Mao, and L. Sun, Investigations of key issues on

- the reproducibility of high- $T_c$  superconductivity emerging from compressed  $\text{La}_3\text{Ni}_2\text{O}_7$ , *Matter and Radiation at Extremes* **10**, 027801 (2025).
- [19] J. Hou, P.-T. Yang, Z.-Y. Liu, J.-Y. Li, P.-F. Shan, L. Ma, G. Wang, N.-N. Wang, H.-Z. Guo, J.-P. Sun, Y. Uwatoko, M. Wang, G.-M. Zhang, B.-S. Wang, and J.-G. Cheng, Emergence of High-Temperature Superconducting Phase in Pressurized  $\text{La}_3\text{Ni}_2\text{O}_7$  Crystals, *Chinese Physics Letters* **40**, 117302 (2023).
- [20] Y. Zhang, D. Su, Y. Huang, Z. Shan, H. Sun, M. Huo, K. Ye, J. Zhang, Z. Yang, Y. Xu, Y. Su, R. Li, M. Smidman, M. Wang, L. Jiao, and H. Yuan, High-temperature superconductivity with zero resistance and strange-metal behaviour in  $\text{La}_3\text{Ni}_2\text{O}_{7-\delta}$ , *Nature Physics* **20**, 1269 (2024).
- [21] C.-Q. Chen, Z. Luo, M. Wang, W. Wú, and D.-X. Yao, Trilayer multiorbital models of  $\text{La}_4\text{Ni}_3\text{O}_{10}$ , *Phys. Rev. B* **110**, 014503 (2024).
- [22] L. Wang, Y. Li, S.-Y. Xie, F. Liu, H. Sun, C. Huang, Y. Gao, T. Nakagawa, B. Fu, B. Dong, Z. Cao, R. Yu, S. I. Kawaguchi, H. Kadobayashi, M. Wang, C. Jin, H.-k. Mao, and H. Liu, Structure Responsible for the Superconducting State in  $\text{La}_3\text{Ni}_2\text{O}_7$  at High-Pressure and Low-Temperature Conditions, *Journal of the American Chemical Society* **146**, 7506 (2024).
- [23] C. D. Ling, D. N. Argyriou, G. Wu, and J. Neumeier, Neutron diffraction study of  $\text{La}_3\text{Ni}_2\text{O}_7$ : Structural relationships among  $n = 1, 2$ , and 3 phases  $\text{La}_{n+1}\text{Ni}_n\text{O}_{3n+1}$ , *Journal of Solid State Chemistry* **152**, 517 (2000).
- [24] J. Yuan, Q. Chen, K. Jiang, Z. Feng, Z. Lin, H. Yu, G. He, J. Zhang, X. Jiang, X. Zhang, Y. Shi, Y. Zhang, M. Qin, Z. G. Cheng, N. Tamura, Y.-f. Yang, T. Xiang, J. Hu, I. Takeuchi, K. Jin, and Z. Zhao, Scaling of the strange-metal scattering in unconventional superconductors, *Nature* **602**, 431 (2022).
- [25] Q.-G. Yang, D. Wang, and Q.-H. Wang, Possible  $s_{\pm}$ -wave superconductivity in  $\text{La}_3\text{Ni}_2\text{O}_7$ , *Physical Review B* **108**, L140505 (2023).
- [26] Y. Shen, M. Qin, and G.-M. Zhang, Effective Bi-Layer Model Hamiltonian and Density-Matrix Renormalization Group Study for the High- $T_c$  Superconductivity in  $\text{La}_3\text{Ni}_2\text{O}_7$  under High Pressure, *Chinese Physics Letters* **40**, 127401 (2023).
- [27] Y.-f. Yang, G.-M. Zhang, and F.-C. Zhang, Interlayer valence bonds and two-component theory for high- $T_c$  superconductivity of  $\text{La}_3\text{Ni}_2\text{O}_7$  under pressure, *Phys. Rev. B* **108**, L201108 (2023).
- [28] Y.-B. Liu, J.-W. Mei, F. Ye, W.-Q. Chen, and F. Yang,  $s_{\pm}^{\pm}$ -wave pairing and the destructive role of apical-oxygen deficiencies in  $\text{La}_3\text{Ni}_2\text{O}_7$  under pressure, *Phys. Rev. Lett.* **131**, 236002 (2023).
- [29] Z. Luo, B. Lv, M. Wang, W. Wú, and D.-X. Yao, High- $T_c$  superconductivity in  $\text{La}_3\text{Ni}_2\text{O}_7$  based on the bilayer two-orbital t-J model, *npj Quantum Materials* **9**, 1 (2024).
- [30] Y. Gu, C. Le, Z. Yang, X. Wu, and J. Hu, Effective model and pairing tendency in the bilayer Ni-based superconductor  $\text{La}_3\text{Ni}_2\text{O}_7$ , *Phys. Rev. B* **111**, 174506 (2025).
- [31] C. Xia, H. Liu, S. Zhou, and H. Chen, Sensitive dependence of pairing symmetry on Ni- $e_g$  crystal field splitting in the nickelate superconductor  $\text{La}_3\text{Ni}_2\text{O}_7$ , *Nature Communications* **16**, 1054 (2025).
- [32] Z. Fan, J.-F. Zhang, B. Zhan, D. Lv, X.-Y. Jiang, B. Normand, and T. Xiang, Superconductivity in nickelate and cuprate superconductors with strong bilayer coupling, *Phys. Rev. B* **110**, 024514 (2024).
- [33] K. Jiang, Z. Wang, and F.-C. Zhang, High-Temperature Superconductivity in  $\text{La}_3\text{Ni}_2\text{O}_7$ , *Chinese Physics Letters* **41**, 017402 (2024).
- [34] Y. Wang, K. Jiang, Z. Wang, F.-C. Zhang, and J. Hu, Electronic and magnetic structures of bilayer  $\text{La}_3\text{Ni}_2\text{O}_7$  at ambient pressure, *Phys. Rev. B* **110**, 205122 (2024).
- [35] Y.-H. Tian, Y. Chen, J.-M. Wang, R.-Q. He, and Z.-Y. Lu, Correlation effects and concomitant two-orbital  $s_{\pm}$ -wave superconductivity in  $\text{La}_3\text{Ni}_2\text{O}_7$  under high pressure, *Phys. Rev. B* **109**, 165154 (2024).
- [36] Y. Zhang, L.-F. Lin, A. Moreo, T. A. Maier, and E. Dagotto, Trends in electronic structures and  $s_{\pm}$ -wave pairing for the rare-earth series in bilayer nickelate superconductor  $\text{R}_3\text{Ni}_2\text{O}_7$ , *Phys. Rev. B* **108**, 165141 (2023).
- [37] J. Huang, Z. D. Wang, and T. Zhou, Impurity and vortex states in the bilayer high-temperature superconductor  $\text{La}_3\text{Ni}_2\text{O}_7$ , *Phys. Rev. B* **108**, 174501 (2023).
- [38] Y.-Y. Zheng and W. Wú,  $s_{\pm}$ -wave superconductivity in the bilayer two-orbital hubbard model, *Phys. Rev. B* **111**, 035108 (2025).
- [39] X.-Z. Qu, D.-W. Qu, J. Chen, C. Wu, F. Yang, W. Li, and G. Su, Bilayer  $t-J-J_{\perp}$  model and magnetically mediated pairing in the pressurized nickelate  $\text{La}_3\text{Ni}_2\text{O}_7$ , *Phys. Rev. Lett.* **132**, 036502 (2024).
- [40] C. Lu, Z. Pan, F. Yang, and C. Wu, Interlayer-Coupling-Driven High-Temperature Superconductivity in  $\text{La}_3\text{Ni}_2\text{O}_7$  under Pressure, *Physical Review Letters* **132**, 146002 (2024).
- [41] Y. Zhang, L.-F. Lin, A. Moreo, T. A. Maier, and E. Dagotto, Structural phase transition,  $s_{\pm}$ -wave pairing, and magnetic stripe order in bilayered superconductor  $\text{La}_3\text{Ni}_2\text{O}_7$  under pressure, *Nature Communications* **15**, 2470 (2024).
- [42] H. Sakakibara, N. Kitamine, M. Ochi, and K. Kuroki, Possible high  $T_c$  superconductivity in  $\text{La}_3\text{Ni}_2\text{O}_7$  under high pressure through manifestation of a nearly half-filled bilayer hubbard model, *Physical Review Letters* **132**, 106002 (2024).
- [43] F. Lechermann, J. Gondolf, S. Bötzel, and I. M. Eremin, Electronic correlations and superconducting instability in  $\text{La}_3\text{Ni}_2\text{O}_7$  under high pressure, *Physical Review B* **108**, L201121 (2023).
- [44] R. Jiang, J. Hou, Z. Fan, Z.-J. Lang, and W. Ku, Pressure driven fractionalization of ionic spins results in cuprate-like high- $T_c$  superconductivity in  $\text{La}_3\text{Ni}_2\text{O}_7$ , *Phys. Rev. Lett.* **132**, 126503 (2024).
- [45] S. Ryeong, N. Witt, and T. O. Wehling, Quenched pair breaking by interlayer correlations as a key to superconductivity in  $\text{La}_3\text{Ni}_2\text{O}_7$ , *Phys. Rev. Lett.* **133**, 096002 (2024).
- [46] G. Heier, K. Park, and S. Y. Savrasov, Competing  $d_{xy}$  and  $s_{\pm}$  pairing symmetries in superconducting  $\text{La}_3\text{Ni}_2\text{O}_7$ : LDA+FLEX calculations, *Phys. Rev. B* **109**, 104508 (2024).
- [47] Z. Liao, L. Chen, G. Duan, Y. Wang, C. Liu, R. Yu, and Q. Si, Electron correlations and superconductivity in  $\text{La}_3\text{Ni}_2\text{O}_7$  under pressure tuning, *Phys. Rev. B* **108**, 214522 (2023).
- [48] D. Varjas, T. O. Rosdahl, and A. R. Akhmerov, Qsymm: algorithmic symmetry finding and symmetric Hamiltonian generation, *New Journal of Physics* **20**, 093026 (2018).
- [49] M. G. Vergniory, L. Elcoro, C. Felser, N. Regnault, B. A.

- Bernevig, and Z. Wang, A complete catalogue of high-quality topological materials, *Nature* **566**, 480 (2019).
- [50] J. Cano and B. Bradlyn, Band Representations and Topological Quantum Chemistry, *Annual Review of Condensed Matter Physics* **12**, 225 (2021).
- [51] F. Tang, H. C. Po, A. Vishwanath, and X. Wan, Comprehensive search for topological materials using symmetry indicators, *Nature* **566**, 486 (2019).
- [52] F. Tang, H. C. Po, A. Vishwanath, and X. Wan, Efficient topological materials discovery using symmetry indicators, *Nature Physics* **15**, 470 (2019).
- [53] B. Bradlyn, L. Elcoro, J. Cano, M. G. Vergniory, Z. Wang, C. Felser, M. I. Aroyo, and B. A. Bernevig, Topological quantum chemistry, *Nature* **547**, 298 (2017).
- [54] F. Tang, H. C. Po, A. Vishwanath, and X. Wan, Towards ideal topological materials: Comprehensive database searches using symmetry indicators, *Nature* **566**, 486 (2019).
- [55] L. Elcoro, B. J. Wieder, Z. Song, Y. Xu, B. Bradlyn, and B. A. Bernevig, Magnetic topological quantum chemistry, *Nature Communications* **12**, 5965 (2021).
- [56] J. Kruthoff, J. de Boer, J. van Wezel, C. L. Kane, and R.-J. Slager, Topological Classification of Crystalline Insulators through Band Structure Combinatorics, *Physical Review X* **7**, 041069 (2017).
- [57] R.-J. Slager, A. Mesaros, V. Juričić, and J. Zaanen, The space group classification of topological band-insulators, *Nature Physics* **9**, 98 (2013), publisher: Nature Publishing Group.
- [58] A. Bouhon, G. F. Lange, and R.-J. Slager, Topological correspondence between magnetic space group representations and subdimensions, *Phys. Rev. B* **103**, 245127 (2021).
- [59] See Supplemental Material at [URL will be inserted by publisher] The standard BdG Hamiltonian used in the main text; the details of the path integral formulation; the details of the original and refined SI groups and the formulas for superconductors; the comprehensive table the symmetry-allowed pairings and the details of the numerical results. The Supplemental Material also contains Refs. [17,48,50,53,55,58,60-64].
- [60] Z. Luo, X. Hu, M. Wang, W. Wú, and D.-X. Yao, Bilayer two-orbital model of  $\text{La}_3\text{Ni}_2\text{O}_7$  under pressure, *Physical Review Letters* **131**, 126001 (2023).
- [61] P. Coleman, Superconductivity and BCS theory, in *Introduction to Many-Body Physics* (Cambridge University Press, 2015) p. 486–541.
- [62] O. Can, T. Tummuru, R. P. Day, I. Elfimov, A. Damascelli, and M. Franz, High-temperature topological superconductivity in twisted double-layer copper oxides, *Nature Physics* **17**, 519 (2021).
- [63] S. Ono, H. C. Po, and H. Watanabe, Refined symmetry indicators for topological superconductors in all space groups, *Science Advances* **6**, eaaz8367 (2020).
- [64] S. Ono, Y. Yanase, and H. Watanabe, Symmetry indicators for topological superconductors, *Physical Review Research* **1**, 013012 (2019).
- [65] S. Ono, Y. Yanase, and H. Watanabe, Symmetry indicators for topological superconductors, *Phys. Rev. Res.* **1**, 013012 (2019).
- [66] A. Skurativska, T. Neupert, and M. H. Fischer, Atomic limit and inversion-symmetry indicators for topological superconductors, *Phys. Rev. Res.* **2**, 013064 (2020).
- [67] T. Bzdušek and M. Sigrist, Robust doubly charged nodal lines and nodal surfaces in centrosymmetric systems, *Physical Review B* **96**, 155105 (2017).
- [68] G.-H. Feng, Nodal higher-order topological superconductivity from  $C_6$ -symmetric dirac semimetals, *Phys. Rev. B* **110**, 174513 (2024).
- [69] S. Coh and D. Vanderbilt, Python tight binding (pythtb) (2022).
- [70] H.-X. Xu, Y. Xie, D. Guterding, and Z. Wang, Competition of superconducting pairing symmetries in  $\text{La}_3\text{Ni}_2\text{O}_7$  (2025).
- [71] S. Ono, K. Shiozaki, and H. Watanabe, Classification of time-reversal symmetric topological superconducting phases for conventional pairing symmetries, *Phys. Rev. B* **109**, 214502 (2024).
- [72] S. Ono, H. C. Po, and K. Shiozaki,  $\mathbb{Z}_2$ -enriched symmetry indicators for topological superconductors in the 1651 magnetic space groups, *Phys. Rev. Res.* **3**, 023086 (2021).
- [73] S. Fan, M. Ou, M. Scholten, Q. Li, Z. Shang, Y. Wang, J. Xu, H. Yang, I. M. Eremin, and H.-H. Wen, Superconducting gaps revealed by STM measurements on  $\text{La}_2\text{PrNi}_2\text{O}_7$  thin films at ambient pressure (2025), arXiv:2506.01788 [cond-mat.supr-con].